

# Distance Preserving Grid Layouts

Gladys M. Hilasaca, Fernando V. Paulovich, *Member, IEEE*

**Abstract**—Distance preserving visualization techniques have emerged as one of the fundamental tools for data analysis. One example is the techniques that arrange data instances into two-dimensional grids so that the pairwise distances among the instances are preserved into the produced layouts. Currently, state-of-the-art approaches produce such grids by solving assignment problems or using permutations to optimize cost functions. Although precise, such strategies are computationally expensive, limited to small datasets, or being dependent on specialized hardware to speed up the process. In this paper, we present a new technique, called Distance-preserving Grid (DGrid), that employs a binary space partitioning process in combination with multidimensional projections to create orthogonal regular grid layouts. Our results show that DGrid is as precise as the existing state-of-the-art techniques, whereas requiring only a fraction of the running time and computational resources, opening up possibilities of applications not previously covered. As an example, we employ the DGrid to organize large photo collections by enabling users to control the semantics of the similarity between photos in real-time.

**Index Terms**—Distance preserving visualization, Grid visualization, Distance preserving grids.

## 1 INTRODUCTION

DISTANCE preserving visualization techniques compose a family of strategies that seek to map data instances into graphical elements so that the pairwise distances calculated between instances are preserved between graphical elements. Among the existing strategies, the multidimensional projections or dimensional reduction techniques have emerged as one of the fundamental tools for data analysis [1]. Through the definition of a proper function to compute the distance between instances, projection techniques produce layouts where the dissimilarity patterns are “visible,” allowing the execution of tasks that involve the identification and analysis of distance relationships.

Despite their popularity, with applications varying from fiber tracking analysis [2] to visual text mining [3], [4], [5], projection techniques present limitations when the graphical elements are used to convey information, tending to produce layouts with overlapped elements. Therefore, suffering from occlusion problems. Some approaches employ post-processing strategies to address such limitation [6], [7] or put constraints on the projection process [8] to remove the overlapping. However, they make poor use of the visual space, creating layouts with empty areas. Aiming at making better use of the available space, distance preserving grid techniques have been devised to arrange the graphical elements into grids, using as much as possible the visual space.

Currently, the state-of-the-art approaches to produce distance-preserving grids solve assignment problems [9], [10] or use permutations to optimize cost functions [11], [12]. Although precise, such strategies are computationally expensive, limited to small datasets, or being dependent on specialized hardware to speed up the process. In this paper, we introduce a novel approach, called *Distance-preserving Grid (DGrid)* that combines multidimensional projection techniques with a space-partitioning strategy to create orthogonal regular distance-preserving grids. Despite its simplicity,

the quality of the produced layouts and the running times render DGrid a very attractive method for large datasets.

In summary, the main contributions of this paper are:

- A novel distance-preserving grid layout technique that presents high-quality regarding distance and neighborhood preservations while running in a fraction of the time of the current state-of-the-art techniques; and
- A framework to explore image collections that allows real-time tuning of the semantics of the similarity between images to match users’ expectations and the navigation of large collections into different levels of detail.

## 2 RELATED WORK

Different approaches have been proposed to create visual representations for conveying distance information. Dimension reduction or projection techniques are well-known examples, such as the classical scaling [13], t-SNE [14], ISOMAP [15], and LAMP [16]. Another example are the techniques that arrange geometric objects on the plane preserving similarity relations while avoiding overlaps, such as RWordle [7], IncBoard [8], ProjSnippet [6], and the UnTangle Maps [17]. It is beyond the scope of this paper to survey all possible techniques for creating distance layouts. Here we focus on strategies that arrange data into orthogonal regular grids preserving similarity relationships.

One technique that can generate distance preserving grids is the Self-Organizing Map (SOM) [18]. SOM is an unsupervised neural network that creates a discretized lower dimension representation of the data by arranging it into a two-dimensional regular spacing hexagonal or rectangular grid. The main drawback is that it can map several data instances to a single grid cell, opening spaces and overlapping instances on the composed grid [9], [10]. The same occurring to its probabilistic counterpart, the Generative Topographic Mapping (GTM) [19]. Spectral Hashing (SH) [20] can also be used (or adapted) to create distance preserving grids. SH creates hashing codes so that the Hamming distance between two codes approach the Euclidean distance between the instances they represent. Thereby, by splitting the code into bins corresponding to the rows and columns of a grid, SH codes can be used to assign data

• G. M. Hilasaca is with Instituto de Ciências Matemáticas e de Computação, University of São Paulo, São Carlos, Brazil.  
E-mail: marlenyh@icmc.usp.br

• F. V. Paulovich is with Faculty of Computer Science, Dalhousie University, Halifax, Canada.  
E-mail: paulovich@dal.ca

instances to grid cells preserving distances. Though a promising strategy, it suffers from the inherent problem of hashing techniques, collisions. Consequently, the produced grids also present opening spaces and overlapping instances. Our technique can also be viewed as a process to assign data instance to grid cells (indexes), but we ensure a non-overlapping constraint so that each instance is mapped to a single cell.

Another technique that can generate distance preserving grids is the NMAP [21]. NMAP is a space-filling technique that, starting from an input projection, creates rectangular arrangements through a bisecting and scaling recursive process. NMAP was designed for creating distance preserving Treemaps [22], but it can be adapted to produce grids if the rectangles' sizes (weights) are all the same. However, due to its binary partition nature, it can only build squared grids that are power-of-two. The numbers of rows and columns are not input parameters for NMAP, and there is no guarantee of producing orthogonal grids with cells of the same size. Our technique relies on a similar binary partition process but, different from NMAP, we use the projection to impose a distance-based ordering among the data instances. This ordering is then used to assign instances to grid cells or indexes. Our output are indexes while NMAP returns rectangles and their positions on the plane. Consequently, we can generate orthogonal grids of any dimension, covering more realistic scenarios where the dataset is not power-of-two in size.

Starting with a random assignment of the data instances to grid cells, the Self-Sorting Map (SSM) [11], [12] technique uses a permutation process, swapping instances between grid cells, aiming at maximizing a cross-correlation function between the distances among data instances and distances among the cells' positions. Since the number of possible permutations is a function of the factorial of data set size, the SSM technique searches for a locally optimal organization. In this process, the grid is split into quadrants and sub-quadrants, and swaps are performed between cells in different (sub)quadrants. Given the binary nature of this process, strategies need to be used to support non-square power-of-two grids [12]. Also, if the number of cells exceeds the number of data instances, it is not possible to control the position of the empty cells. They are (randomly) spread over the grid. Although gaps can be used to improve the quality of a grid [23], in this case, the empty cells are artifacts of the technique that usually reduces the overall quality. In our technique, the empty cells are grouped in one corner of the grid, avoiding such artifacts and resulting in grids with better quality.

The Kernelized Sorting (KS) [10] technique creates distance preserving grids finding a locally optimal solution for a quadratic assignment problem [24]. KS establishes a matrix containing the pairwise distances between the data instances and a matrix containing the pairwise distances between the grid positions. Then a permutation process is applied on the second matrix to approximate, as much as possible, the first one, resulting in a one-to-one matching between instances and the grid cells. The IsoMatch [9] also employs an assignment strategy for constructing distance preserving grids. First, it projects the data into the plane using the ISOMAP [15] technique and builds a complete bipartite graph between the projection and grid positions. Then, using the Hungarian algorithm [25], it calculates a bipartite matching of this graph, assigning each instance to a grid position to minimize the aggregate displacement when transforming the projection positions into the grid positions. Different from the previous techniques, the KS and the IsoMatch are not limited to rectangular grids.

They can create grids with arbitrary shapes. However, since they solve assignment problems, they are computationally expensive, not being able to handle large datasets or even small datasets in real-time. Our technique, although not supporting arbitrary grids, it is limited to orthogonal ones, can process much larger datasets in a fraction of the time without asking for particular hardware.

Other techniques share similarities with the approach proposed in this paper. For instance, the Rectangular Cartograms [26], [27] scales areas of geographical regions to rectangular shapes in proportion to some statistic, the Tile Maps [28] displays geographic regions as a grid of identical cell sizes, the Origin-Destination maps [29] divides the geographic space into a regular grid and represent trajectories using grid cells, and the point set matching maps [30] assigns centroids of geographical regions to grid cells. Although visually similar, they were not designed to create distance preserving grids, and usually can only handle small datasets due to the high computational complexity, so out of the scope of this paper. Another example that is also visually similar is the work by Meulemans et al. [23], which positions small multiples into a grid optimizing multiple metrics while intentionally add spaces to improve user perception. Such technique could be potentially adapted to generated distance preserving grids, but, as discussed by the authors, new metrics need to be defined since some of the designed ones are not transferable to such application scenario.

### 3 DISTANCE-PRESERVING GRID (DGRID)

#### 3.1 Overview

Given a  $m$ -dimensional dataset  $\mathcal{D} = \{d_1, d_2, \dots, d_N\} \in \mathbb{R}^m$ , and a two-dimensional rectangular grid  $\mathcal{G} = \{g_1, g_2, \dots, g_{r \times s}\}$  composed of  $r$  rows and  $s$  columns, with  $r \times s \geq N$ , distance-preserving grid techniques aim to assign each instance  $d_i$  to a grid cell  $g_i$  so that similar instances are placed on close cells and dissimilar ones on far apart ones. More formally, such techniques work to maximize a given function that represents the rank-order correlation between data instances and grid cells, such as the cross-correlation

$$CC = \frac{1}{N^2} \sum_i^N \sum_j^N \frac{(\lambda(g_i, g_j) - \bar{\lambda})(\delta(d_i, d_j) - \bar{\delta})}{\sigma_\lambda \sigma_\delta} \quad (1)$$

where  $\delta(d_i, d_j)$  is the dissimilarity between pairs of instances,  $\lambda(g_i, g_j)$  is the distance between cells,  $\bar{\lambda}$  is the mean distance between any two cells,  $\bar{\delta}$  is the mean distance between any two pairs of instances, and  $\sigma_\lambda$  and  $\sigma_\delta$  are the corresponding standard deviations. In other words, distance-preserving grid techniques seek to maximize how well the placements (on the grid) of the data instances, as a whole, correlate to the distances among them [12].

Our technique, the *Distance-preserving Grid (DGrid)*, employs a two-step approach to address this optimization problem. In the first step, the data instances are mapped into two-dimensional points  $\mathcal{P} = \{p_1 = (x_1, y_1), \dots, p_N = (x_N, y_N)\} \in \mathbb{R}^2$  using a multi-dimensional projection technique, preserving, as much as possible, the pairwise distances in  $\mathcal{D}$ . Then, a partition scheme is employed to assign each projected point  $p_i$  into a grid cell  $g_i$ , maximizing the rank-order correlation with  $\mathcal{P}$ . The reasoning behind our approach is that if the projection  $\mathcal{P}$  precisely preserves the pairwise distances in  $\mathcal{D}$ , and if  $\mathcal{G}$  preserves the rank-order of the distances in  $\mathcal{P}$ ,  $\mathcal{G}$  will preserve, up to an extent, the rank-order of the distances in  $\mathcal{D}$ . Following, we detail this approach.

### 3.2 Assigning Points to Grid Cells

Considering that each data instance  $d_i \in \mathcal{D}$  has already been mapped into a point  $p_i \in \mathcal{P}$  (later discussed in Section 3.3), the next step is to assign each  $p_i$  into a cell  $g_i \in \mathcal{G}$ . In other words, the next step is to calculate the cell indexes (row and column) for each data instance, preserving the rank-order. For a target grid  $\mathcal{G}$  of dimension  $(r, s)$  ( $r$  rows and  $s$  columns), this process is rather trivial if the marginal distribution of the  $x$ -coordinates of the points in  $\mathcal{P}$  is uniform considering a histogram with  $s$  bins, and the marginal distribution of the  $y$ -coordinates is also uniform but considering a histogram with  $r$  bins. If such distribution holds, the points are distributed following the grid pattern, and it is only necessary to vertically split the projection into  $s$  partitions, with  $r$  instances in each, defining the column index of the instances in each partition. Then, horizontally split the partitions so that each instance is placed in an individual partition, defining the row index of each point or data instance.

Notice that, not only that is a trivial case to solve, but also, this distribution results in the smallest displacement of the points in  $\mathcal{P}$  when assigning them to grid cells on the plane. Therefore approximating  $\lambda(g_i, g_j)$  to  $\delta(p_i, p_j) \forall p_i, p_j \in \mathcal{P}$ , matching the general goal of preserving the rank-order correlation when creating a grid (see Equation (1)). In practice, however, this uniform distribution constraint seldom holds, and the projected points are spread on the plane following more complex patterns. To address this problem, we recursively bisect the projection into non-overlapping partitions until the obtained partitions individually obey such constraint, and (sub)grids are derived from each partition composing the entire grid  $\mathcal{G}$ .

Consider  $\mathcal{P}$  as the input projection with  $N$  instances, and  $\mathcal{G}$  the target grid with  $r$  rows and  $s$  columns. For the first bisection, we have  $r - 1$  different options for horizontal splits and  $s - 1$  for vertical splits. So the question is how to select the best bisection, or the sequence of horizontal and vertical bisections, that produces the largest partitions obeying the uniform distribution constraint. This is a combinatorial problem to solve, impractical for large datasets. Instead, we use the simple idea of splitting the projection in half in the direction (vertical or horizontal) with more rows or columns. In this way, without any expensive test, we increase our probability of getting the largest partitions that obey the uniform distribution constraint – if the number of points in one partition decreases, this probability increases; however, reducing such probability for the other partition; therefore half is a good natural tradeoff.

Thereby, in our process, if  $r > s$ , we split  $\mathcal{P}$  horizontally, obtaining two partitions  $\mathcal{P} = \mathcal{P}_1 \cup \mathcal{P}_2$ , so that, the upper partition  $\mathcal{P}_1$  contains enough instances to completely fill half of the target grid, that is,  $|\mathcal{P}_1| = \lceil r/2 \rceil \times s$ . Otherwise, we split  $\mathcal{P}$  vertically, so that the left partition  $\mathcal{P}_1$  contains enough instances to completely fill half of the target grid, that is,  $|\mathcal{P}_1| = r \times \lceil s/2 \rceil$ . This bisecting process is recursively applied to the resulting partitions until obtaining partitions obeying the uniform distribution constraint. In fact, for partitions following the uniform distribution constraint, this bisecting process will result in the same grid as if we apply the trivial process of calculating indexes. Therefore, instead of penalizing the running time of our approach, adding the uniform constraint test, we execute the bisecting until each partition contains only one instance, rendering a much faster and simpler process to implement.

The last piece of our approach is how to calculate the grid cells' indexes as the projection is partitioned. Consider that the

first bisection splits  $\mathcal{P}$  into  $\mathcal{P}_1$  and  $\mathcal{P}_2$ , where  $\mathcal{P}_1$  is the upper partition for a horizontal bisection or the left partition for a vertical bisection. One way to understand this partitioning process is to think that we are transforming our problem of creating one grid with  $r$  rows and  $s$  columns into a problem of creating two grids with  $s/2$  columns and  $r$  rows for a vertical split or  $r/2$  rows and  $s$  columns for a horizontal one. Without loss of generality, consider that the first bisection vertically splits the input projection  $\mathcal{P}$ . By construction, the index of the most-left column of the grid resulting from  $\mathcal{P}_1$  is 0, and the index of the most-left column of the grid resulting from  $\mathcal{P}_2$  is  $\lceil s/2 \rceil$ . Similarly, for a horizontal split, the index of the most-top row of the grid resulting from  $\mathcal{P}_1$  is 0, and the index of the most-top row of the grid resulting from  $\mathcal{P}_2$  is  $\lceil r/2 \rceil$ . In the general case, given an input partition (projection) to be assigned to a grid with  $r'$  rows and  $s'$  columns. If  $(i, j)$  is the index of the top-left corner cell of the resulting grid, the index of the top-left corner grid cell for  $\mathcal{P}_1$  is  $(i, j)$ , and the index of the top-left corner grid cell for  $\mathcal{P}_2$  is  $(i + \lceil r'/2 \rceil, j)$  for a horizontal cut, and  $(i, j + \lceil s'/2 \rceil)$  for a vertical cut. If the input partition has only one point,  $(i, j)$  is the cell index to which the single point is assigned.

Figure 1 depicts this process. In this example, a projection with 20 points following a non-uniform marginal distribution (Figure 1(a)) is assigned to a grid with 4 rows and 5 columns. Since such a grid has more columns than rows, the first bisection is vertical (Figure 1(b)). The resulting left partition contains enough points to fill half of the final grid, that is, 4 rows and 3 columns, and the top-left corner grid cell of the resulting (sub)grid receives the index  $[0, 0]$ . The right partition contains the remaining points, and the top-left corner grid cell receives the index  $[0, 3]$ . Next, the right partition is bisected (Figure 1(c)). Since the (sub)grid resulting from this partition has more rows than columns, it is horizontally split. Again, each resulting partition receives half of the points, so that both will result in grids with 2 rows and 3 columns. The top-left corner cell of the resulting grid from the upper partition receives the index  $[0, 0]$ , whereas the top-left corner cell of the resulting grid from the lower partition receives the index  $[2, 0]$ . This partitioning process is then recursively applied to the resulting partitions until each partition contains only one point (Figure 1(h)). In Figure 1(h), we are not showing the index of some partitions to avoid cluttering the image. Also, notice that, since the goal is to create a grid with a given number of rows and columns, the bisecting process is not a simple alternating process between vertical and horizontal cuts, and successive cuts can occur in the same direction (Figure 1(e)).

Algorithm 1 puts all these pieces together, showing the overall process adopted by our approach to assigning a projection to a grid. The function  $\text{SPLIT}_y(\mathcal{P}, k)$  performs the horizontal bisection. In this process,  $\mathcal{P}$  is sorted according to the  $y$ -coordinates ( $\mathcal{P}$  is viewed as a list). The first  $k$  instances are assigned to  $\mathcal{P}_1$  and the remaining to  $\mathcal{P}_2$ . The function  $\text{SPLIT}_x(\mathcal{P}, k)$  performs the vertical bisection using the same process, but sorting  $\mathcal{P}$  according to the  $x$ -coordinates. Notice that since the bisecting process always assigns to the upper and left partitions enough elements to result in a filled grid, spaces are not opened in the interior of the final grid. All empty cells are grouped on the bottom-right corner.

A different interpretation of this binary partition method is to consider it as a translation process that removes void spaces so that the distribution of the projected points on the vertical and horizontal directions is as uniform as possible and follows the grid dimensions, that is, the desired number of rows and columns. Since translation

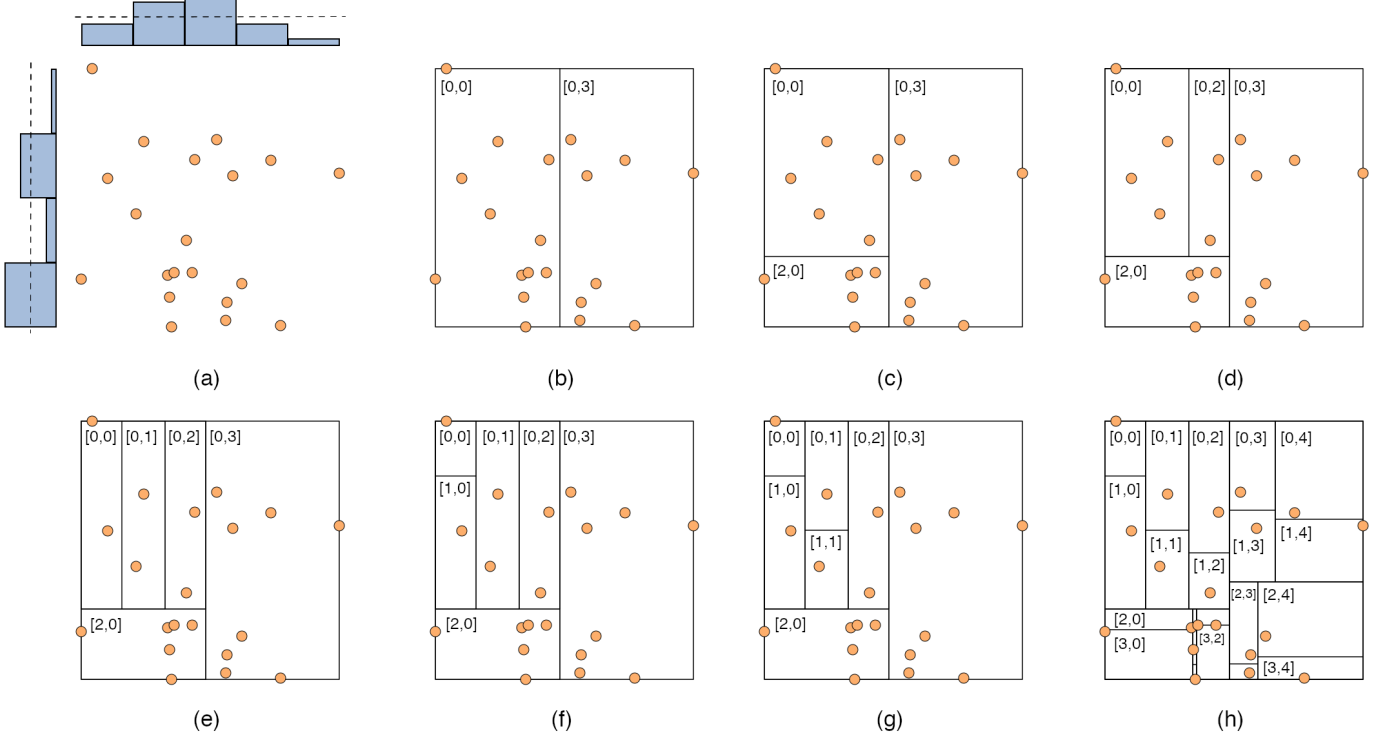


Fig. 1. Process of assigning points to grid cells. In this example, a projection with 20 points following a non-uniform marginal distribution (a) is assigned to a grid with 4 rows and 5 columns. Starting from a vertical cut (b), the projection is recursively split until each partition contains only one point, resulting in the grid cell indexes (h).

#### Algorithm 1 Process of calculating the indexes of the grid cells.

**Require:**  
 $\mathcal{P} = \{p_1, p_2, \dots, p_N\}$  the input projection  
 $(r, s)$  the grid dimension (number of rows and columns)

```

function DGRID( $\mathcal{P}, (r, s)$ )
     $\mathcal{G} \leftarrow \mathcal{P}$             $\triangleright$  Assign to each  $g_i \in \mathcal{G}$  coordinates of  $p_i \in \mathcal{P}$ 
    return DGRID_AUX( $\mathcal{G}, (r, s), (0, 0)$ )
end function

function DGRID_AUX( $\mathcal{G}, (r, s), (i, j)$ )
    if  $\mathcal{G} \neq \emptyset$  then
        if  $|\mathcal{G}| = 1$  then            $\triangleright \mathcal{G}$  has one instance
             $g_1 \leftarrow (i, j)$        $\triangleright$  cell  $g_0 \in \mathcal{G}$  receives the index  $(i, j)$ 
        else
            if  $r > s$  then
                 $\mathcal{G}_1, \mathcal{G}_2 \leftarrow \text{SPLIT}_y(\mathcal{G}, \min(|\mathcal{G}|, \lceil r/2 \rceil \times s))$ 
                 $\mathcal{G}_1 \leftarrow \text{DGRID\_AUX}(\mathcal{G}_1, (\lceil r/2 \rceil, s), (i, j))$ 
                 $\mathcal{G}_2 \leftarrow \text{DGRID\_AUX}(\mathcal{G}_2, (r - \lceil r/2 \rceil, s), (i + \lceil r/2 \rceil, j))$ 
                return  $\mathcal{G}_1 \cup \mathcal{G}_2$ 
            else
                 $\mathcal{G}_1, \mathcal{G}_2 \leftarrow \text{SPLIT}_x(\mathcal{G}, \min(|\mathcal{G}|, r \times \lceil s/2 \rceil))$ 
                 $\mathcal{G}_1 \leftarrow \text{DGRID\_AUX}(\mathcal{G}_1, (r, \lceil s/2 \rceil), (i, j))$ 
                 $\mathcal{G}_2 \leftarrow \text{DGRID\_AUX}(\mathcal{G}_2, (r, s - \lceil s/2 \rceil), (i, j + \lceil s/2 \rceil))$ 
                return  $\mathcal{G}_1 \cup \mathcal{G}_2$ 
            end if
        end if
    end if
return  $\mathcal{G}$ 
end function

```

is a rigid transformation that preserves relative distances, in the worst-case scenario, half of the distance relationships are fully kept when a projection is bisected. Typically, more than that is preserved, so that  $\mathcal{G}$  preserves the rank-order of distances in  $\mathcal{P}$ , consequently, preserving, up to an extent, the distances relationships in  $\mathcal{D}$ .

### 3.3 Projecting the Dataset

As mentioned, the first step of our approach consists of mapping the dataset  $\mathcal{D}$  into  $\mathcal{P}$ . Given the general goal of preserving the rank-order correlation when creating a grid (see Equation (1)), if  $d(p_i, p_j)$  is the distance between points in  $\mathcal{P}$ , such mapping should minimize  $\sum_i \sum_j (\delta(d_i, d_j) - d(p_i, p_j))$ . In the current literature, there are several multidimensional projection techniques that can be employed to this end. Typically, the most precise techniques, such as the classical multidimensional scaling [13] or the t-SNE [14], are computationally expensive, whereas the less precise out-of-sample methods, such as LAMP [16] or PLMP [31], can handle very large datasets in a reasonable amount of time. Another aspect to consider is global versus local distance preservation, that is, if the goal is to preserve pairwise distances between all instances or only between instances in small neighborhoods. This is an important aspect since projections serve as proxies to the rank-order of the pairwise distances in  $\mathcal{D}$ , and the resulting grid will reflect the different properties preserved by them. Thereby, the choice of what technique to use relies on the tradeoff between the size of the dataset and the desired precision, and also if local or global preservation is preferred (check [1] for a further discussion on techniques' properties). In this paper, we use two different techniques, LAMP and t-SNE, to show the flexibility of our approach to derive grids that preserve different properties and can handle large datasets.

Regardless of the employed method, distance preserving projections are invariant to rigid transformations. Therefore, better

or more precise grids could be attained by simply rotating the input projection. Since our approach recursively bisects the projection, generating different partitions every recursion, the only way to find the rotation that maximizes the cross-correlation (see Equation 1), would be to rotate the projection considering different angles, applying the assignment procedure, and measuring the cross-correlation. This is a prohibitive process (only the cross-correlation is quadratic to compute), so we approximate it by getting the rotation that best approaches the  $x$ -coordinates and  $y$ -coordinates marginal distributions to uniformity. Given a target grid with  $r$  rows and  $s$  columns, for each different rotation, we calculate the standard deviation  $std_x$  of the histogram with  $s$  bins for the  $x$ -coordinates, and the standard deviation  $std_y$  of the histogram with  $r$  bins for the  $y$ -coordinates. The best rotation is the one that minimizes  $std_x \times std_y$  (we uniformly rotate the projection between  $0^\circ$  and  $90^\circ$ ). Notice that this is a global criterion, and, although it has shown to be a good approximation, there is no guarantee that it will find the best rotation.

### 3.4 Grid Dimension

The process of assigning a projection to a grid defined in the previous section is very flexible. Since it focuses on splitting the partitions considering the number of rows and columns, instead of the number of data instances, it is not limited to any particular grid aspect-ratio. The only constraint is that the number of grid cells should be bigger or equal to the number of data instances, that is,  $r \times s \geq N$ .

In this paper, we allow the control of the grid dimensions by defining its aspect-ratio  $\Delta$ . Here,  $\Delta$  is the ratio between the number of rows and the number of columns, or the ratio between the height and width of the visual space. Given  $\Delta$ , the target grid dimension is calculated as

$$\begin{aligned} r &= \lfloor \sqrt{N * \Delta} \rfloor \\ s &= \lceil N/r \rceil \end{aligned} \quad (2)$$

with  $N \geq \Delta \geq 1$ . If  $\Delta = 1$ , the resulting grid will be as square as possible. If  $1 < \Delta \leq N$ , the resulting grid will have  $\Delta$  times more rows than columns. If  $0 < \Delta < 1$ , the resulting grid will have  $1/\Delta$  times more columns than rows.

## 4 RESULTS

### 4.1 Evaluation and Comparison

In this section, we present a quantitative evaluation of the *Distance-preserving Grid (DGrid)* technique, comparing it against the state-of-the-art in distance preservation grid techniques, viz., Kernelized Sorting (KS) [10], Self-Sorting Map (SSM) [12], and IsoMatch [9]. In this comparison we use three different quality metrics, cross-correlation [12],  $k$ -neighborhood preservation index [32], and energy function [9]. The cross-correlation (see Equation 1) measures how well the placements of the data instances in the grid correlate to the dissimilarities among them. It ranges in  $[-1, 1]$ , the larger the better. In this paper, we normalize the cross-correlation in  $[0, 1]$  using  $CC' = (CC + 1)/2$  to ease the comparison among the different metrics. The  $k$ -neighborhood preservation index was originally developed to evaluate projections, but here we use it to measure how much the neighborhood in the dataset  $\mathcal{D}$  is preserved in the grid  $\mathcal{G}$ . It is calculated as

$$NP_k = \frac{1}{N} \sum_i^N \frac{|N_{k_i}^{\mathcal{D}} \cap N_{k_i}^{\mathcal{G}}|}{k} \quad (3)$$

where  $N_{k_i}^{\mathcal{X}}$  is the set containing the indexes of the  $k$ -nearest neighbors of  $d_i$  in  $\mathcal{D}$ , and  $N_{k_i}^{\mathcal{G}}$  is the set containing the indexes of the  $k$ -nearest neighbors of  $g_i$  in  $\mathcal{G}$ .  $NP_k$  ranges in  $[0, 1]$ , the larger the value the better the result. Finally, the energy function measures how well the pairwise distances between the data instances are preserved by the corresponding distances in the grid. This function is computed as

$$E_p = \left( \sum_i^N \sum_j^N \frac{|c \cdot \delta(d_i, d_j) - \lambda(g_i, g_j)|^p}{\sum_r^N \sum_s^N \lambda(g_r, g_s)^p} \right)^{\frac{1}{p}} \quad (4)$$

where  $p$  defines the employed norm, and  $c$  is a scaling constant (see [9] for more details). As suggested in [9], we set  $p = 1$  since it favors solutions which preserve the smaller distances more than the larger ones. Also, we invert the original equation using  $E'_p = 1 - E_p$  so that it ranges in  $[0, 1]$  with larger values rendering better results.

For the tests, we have selected all datasets from the *UCI Machine Learning Repository* [33] with real-valued attributes and sizes varying between 100 and 2,500 instances, allowing the comparison of the techniques in different scenarios. We only get real-valued datasets so that (Euclidean) distances can be properly calculated, and we limited their sizes due to the high computational complexities and running times of KS and IsoMatch techniques. Also, we have discarded the datasets with missing values, resulting in 38 datasets. The first part of Table 1 details these datasets, presenting their names, sizes, and number of dimensions. For all tests, we have normalized the datasets so that the columns (attributes) have zero mean and standard deviation equals to one. All the results were generated in an Intel Core i7 CPU@2.8GHz, with 16GB of RAM. For the SSM, KS, and IsoMatch techniques, we used the original codes made available by the authors.

Figure 2 presents boxplots summarizing the results of each technique considering all the 38 datasets. For the DGrid, we report results using t-SNE and LAMP techniques to generate the input projections. Given that projections are invariant to rotation, we employ the devised process presented in Section 3.3, rotating the input projections 20 times to get the layout that minimizes the standard deviation of the marginal histograms. Although the IsoMatch originally employs the ISOMAP as input, we also report results using t-SNE and LAMP, so it is possible to compare the DGrid and the IsoMatch isolating the projection contribution to the quality of the produced results. The DGrid, IsoMatch, and KS techniques are deterministic, so we only run each technique once for each dataset. Given the random initialization of the SSM technique, we run it 30 times for each dataset. In Figure 2, the boxplots in red represent the results of the projections (LAMP and t-SNE) used as input by DGrid and IsoMatch techniques. They serve only as baselines to show the correlation between projection quality and grid quality. Notice that the drop in precision between the projections and the produced grids is expected since the techniques we use do not create uniformly distributed projections (see Section 3). Also note that direct comparisons only make sense among grid layouts, not among grids and projections.

Regarding the  $k$ -neighborhood preservation index (Figure 2(a)), on average, the best result was attained by the DGrid with t-SNE as input ( $\overline{NP} = 0.53$ ), better than the SSM ( $\overline{NP} = 0.41$ ) and the other more costly counterparts, IsoMatch ( $\overline{NP} = 0.36$ ) and KS ( $\overline{NP} = 0.50$ ). Also, DGrid presents the smallest spread regarding the best and worst results. Comparing the different flavors of DGrid, the results produced using t-SNE are considerably superior

TABLE 1

Datasets employed in the evaluations. We have selected all datasets from the *UCI Machine Learning Repository* with real-valued attributes and sizes up to a limit, allowing the comparison of the techniques in different scenarios.

Name	Size	Dimensions
Concrete Slump Test	103	10
Breast Tissue	106	10
LSVT Voice Rehabilitation	126	309
Iris	150	4
Urban Land Cover	168	148
Planning Relax	182	13
Parkinsons	197	23
Connectionist Bench	208	60
Seeds	210	7
Glass Identification	214	10
Yacht Hydrodynamics	308	7
Vertebral Column	310	6
Ecoli	336	8
Leaf	340	16
Libras Movement	360	91
PEMS	440	138,672
Forest Fires	517	11
Vowel Recognition	528	10
Istanbul Stock Exchange	536	8
Climate	540	18
WDBC	569	32
DrivFace	606	6,400
Hill-Valley	606	100
Blood Transfusion	748	5
Gene Expression	801	20,531
Arcene	900	10,000
MicroMass	931	1,300
Cloud	1,024	10
Concrete Compressive Strength	1,030	9
Geographical Original of Music	1,059	68
Banknote Authentication	1,372	5
Yeast	1,484	8
Airfoil Self-Noise	1,503	5
Plant species leaves	1,600	64
Drug Consumption	1,885	32
Cardiotocography	2,126	23
Image Segmentation	2,100	19
Statlog (Image Segmentation)	2,310	19
HTRU2	17,898	9
Default of credit card	30,000	23
Online News Popularity	39,644	61
Facebook Comments	40,949	54
Tamilnadu Electricity Board	45,781	4
Sensorless Drive Diagnosis	58,509	49
Corel Image Features	68,040	89
Blog Feedback	56,497	281
FMA: A Dataset For Music Analysis	106,574	518
MiniBooNE Particle Identification	130,065	50

to the results produced using LAMP. This is an expected outcome since the formulation of t-SNE favors the preservation of small neighborhoods instead of global distance preservation, as conveyed by LAMP. This is confirmed by the boxplots of the projections in red. This indicates the impact of the input projection on the produced grid, and also shows that our strategy for assigning the projection to grid cells satisfactorily preserves the input geometry. In this example, we approximate the neighborhood size  $k$  to 5% of the dataset size, setting  $k = (\lfloor \sqrt{0.05 * N} \rfloor)^2$ . We use this approximation instead of 5% to match the grid topology when calculating the neighborhoods.

Figure 2(b) shows the cross-correlation results. On average, DGrid with LAMP ( $\overline{CC} = 0.80$ ) presents better results than SSM ( $\overline{CC} = 0.70$ ), IsoMatch ( $\overline{CC} = 0.78$ ) and KS ( $\overline{CC} = 0.78$ ), with a smaller spread regarding the best and worst results. Different from the  $k$ -neighborhood preservation index, which is a local

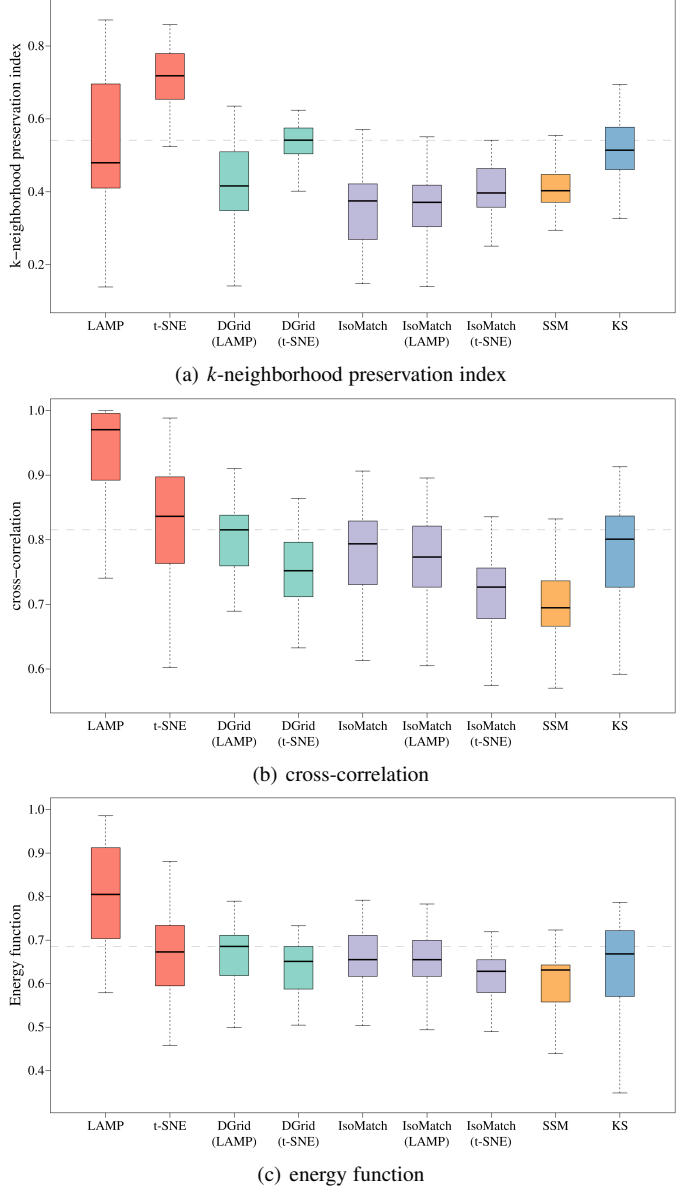


Fig. 2. Boxplots of  $k$ -neighborhood preservation index, cross-correlation, and energy function. In all these aspects, the DGrid surpass (on average) current state-of-the-art techniques, indicating its quality on preserving distance relationships. The boxplots in red summarize the results of the input projection and serve as baselines to show the correlation between projections and grid properties. They are not intend for direct comparisons.

measure, the cross-correlation is global, explaining why the results considering LAMP as input are better than the ones considering t-SNE, which is also confirmed by the projection boxplots in red. This renders exceptional flexibility to our technique since it allows selecting a projection technique that fulfills specific needs, considering different global or local geometry properties, generating grids that suitably preserve them.

The quality of our approach is also confirmed by the energy function metric (Figure 2(c)). The DGrid with LAMP ( $\overline{E_p} = 0.65$ ) again outperforms the other techniques, SSM ( $\overline{E_p} = 0.59$ ), IsoMatch ( $\overline{E_p} = 0.63$ ) and KS ( $\overline{E_p} = 0.63$ ). Since the energy function is a global measure, LAMP technique presents better results than t-SNE (see the red boxplots), which reflects in the produced grids. In [9], the authors show that the energy function strongly correlates with human performance in search tasks, pointing out that this

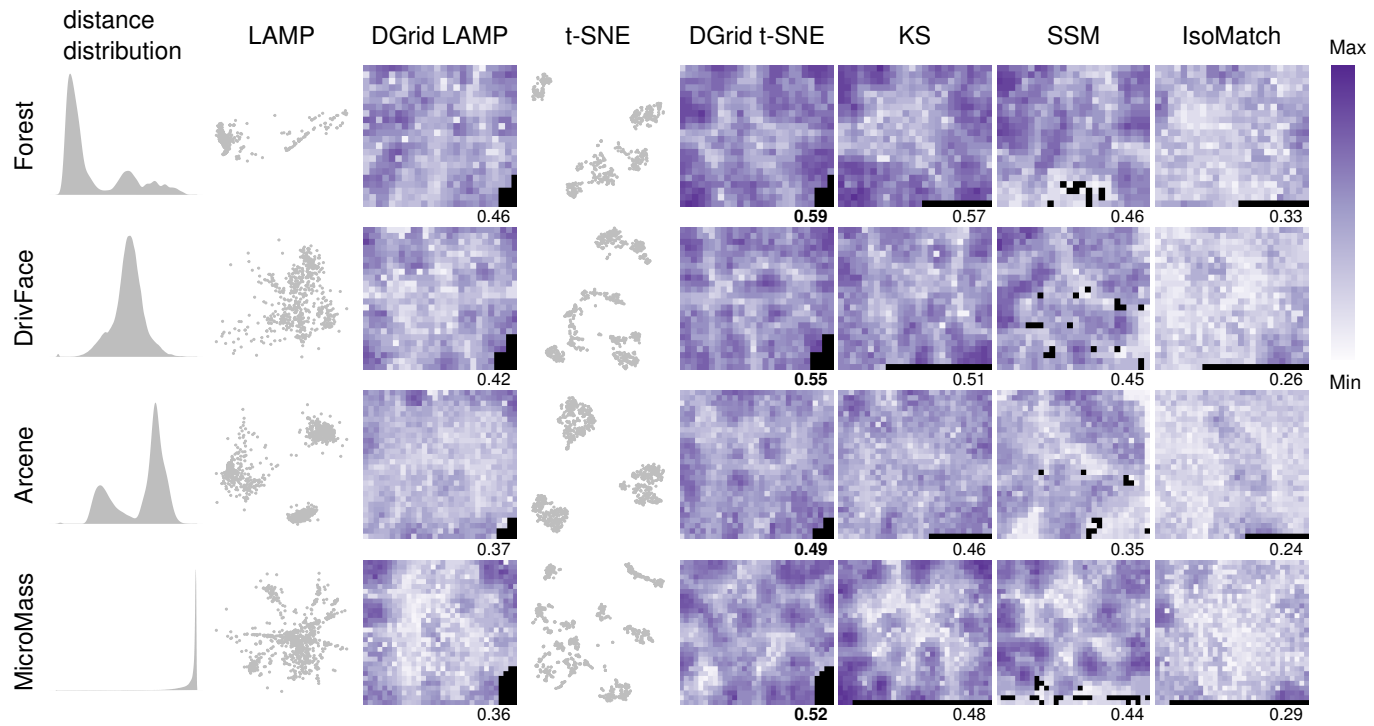


Fig. 3. Resulting grids colored according to the **k-neighborhood preservation index**. SSM technique groups bad quality cells close to the empty cells, showing the negative impact of empty spots on the produced layouts.

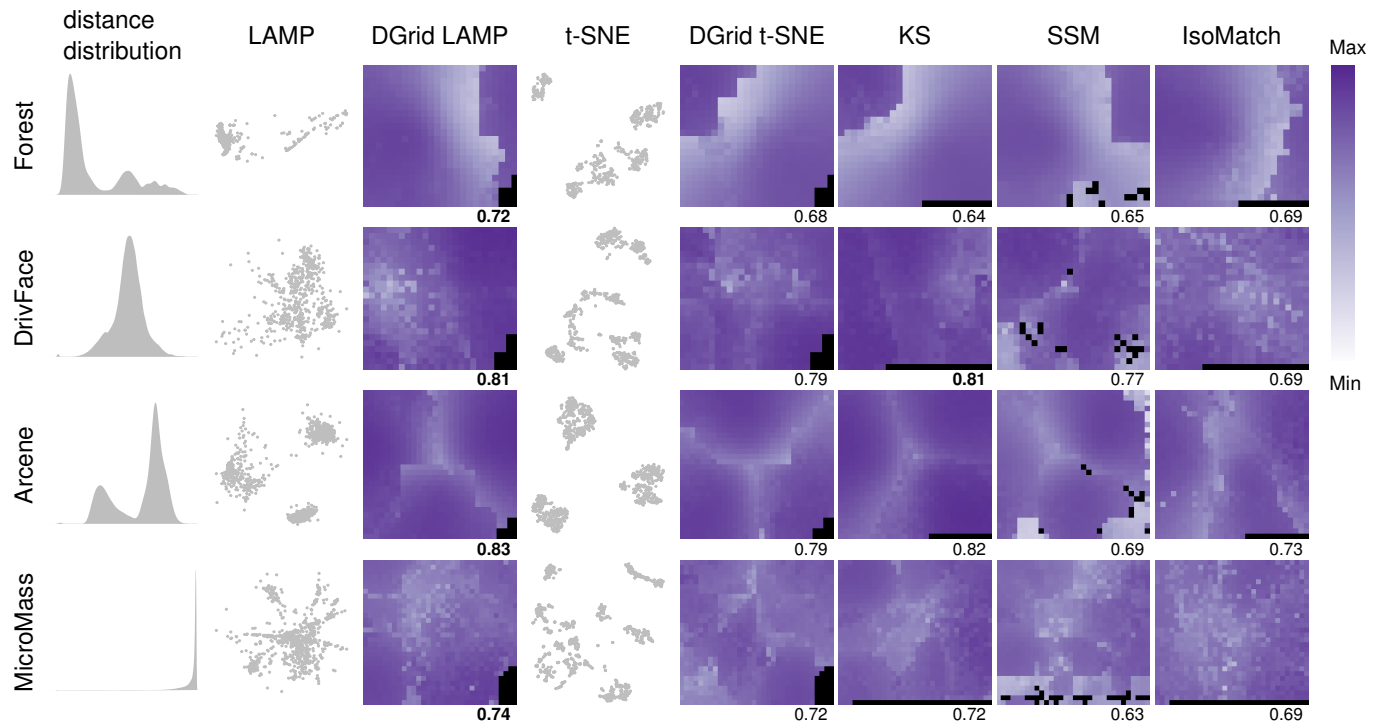


Fig. 4. Resulting grids colored according to the **cross-correlation**. Cross-correlation is global measure, so the use of a global projection technique (LAMP) as input resulted in better grids in that aspect. This renders exceptional flexibility to our approach since it allows selecting a projection technique that fulfills specific geometry properties, generating grids that satisfactorily preserve them.

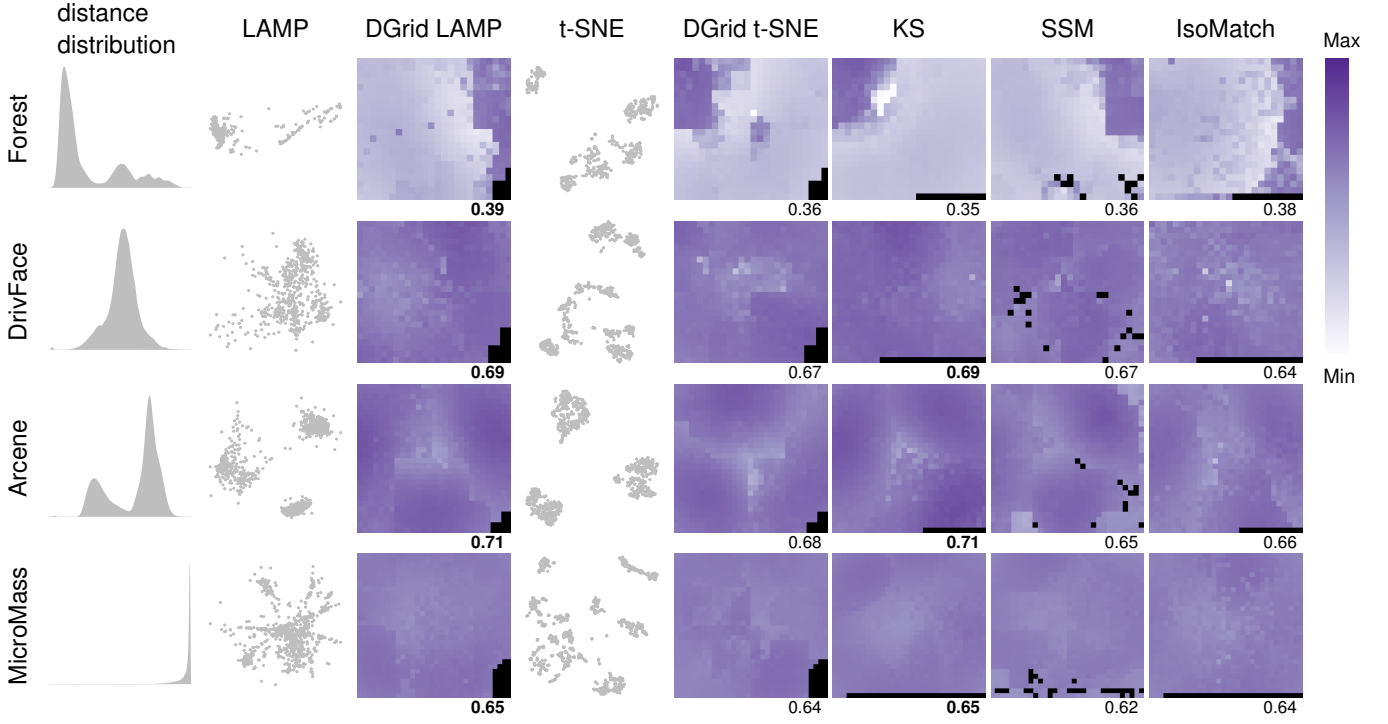


Fig. 5. Resulting grids colored according to the **energy function**. The energy function strongly correlates with human performance in search tasks, placing DGrid among the best choices for tasks that involve the analysis of similarity relationships based on grids.

is a good measure of grid organization. The same holds for the cross-correlation measure. Therefore, the attained results provide evidence to place the combination of DGrid with LAMP as one of the best choices for tasks that involve the analysis of similarity relationships based on grids.

To complement the statistical analysis conveyed by the boxplots, providing more detailed information, we show in Figures 3, 4, and 5 the resulting grids for some selected datasets. Aiming at showing different aspects of each technique, we choose datasets with varied distance distributions, from a dataset with most instances similar among themselves (Forest) to a dataset with most instances dissimilar among themselves (MicroMass). In these figures, the cells are colored according to different quality metrics calculated for each cell. The cells colored in black are empty. They exist because we have more cells than instances in these examples. The quality metric values are shown below each grid, and the best results are highlighted using a bold font. Finally, we also show the input projections used by DGrid to exemplify how projections are mapped to the final grid.

Regarding the  $k$ -neighborhood preservation index grids (Figure 3), the KS and the DGrid with t-SNE, which attained the best results on average (see Figure 2), do not present spots concentrating bad quality cells, the error is uniformly spread over the grid. Conversely, SSM tends to group the bad quality cells close to the empty cells, showing their negative impact on the produced layouts. The cross-correlation grids (Figure 4) report an intriguing pattern produced by all techniques. For the Forest dataset, there is a clear spot with bad quality cells, concentrated in the border of two different regions. A close examination explains the reason. Since the Forest dataset is composed of two very distinct groups of instances, approaching them in the produced layout increases the error in the border cells, an inevitable aspect of grid layouts. A similar result can be observed for the Arcene dataset, which is

composed of 3 distinct groups. The energy function grids (Figure 5) also present an unusual pattern regarding the Forest dataset. The two different groups of instances can be identified, but in these grids, the larger group presents significantly worse results if compared to the smaller one (compare with Figure 4). In this case, the problem is related to the size of the groups. Since one group is much larger than the other, considering the groups individually defines two different scenarios regarding distance distribution. For the smaller group, most instances are dissimilar between themselves, but for the larger, most instances are similar between themselves. Since the energy function is global and measures distance preservation, the differences in distribution affect the quality of the grid cells. Although in these examples, KS presents similar quality as DGrid in some cases, it is an  $O(N^3)$  technique and cannot address problems involving large datasets. DGrid is much less expensive (see Section 6), being able to handle datasets neither KS nor IsoMatch are capable of.

Given the process we develop to derive grids from projections, our approach can obtain better results if the number of rows and columns, controlled by  $\Delta$ , is defined considering the distribution of the input projections. Figure 6 shows the impact of varying  $\Delta$  into the quality of the produced grids. To have better control of this test, we artificially generate a projection with three times more points in the vertical direction than in the horizontal direction. As expected, the best results are attained when  $\Delta = 3$  (the dashed line). In all examples in this section, we have used squared grids, setting  $\Delta = 1$ . Since most techniques we are comparing to do not depend on projections, we prefer to set a fixed value instead of using the best possible value of  $\Delta$  not to bias the evaluation favoring our approach.

Finally, we have compared DGrid with SSM regarding the running times. We have removed the other techniques from this comparison since they are computationally expensive, not capable

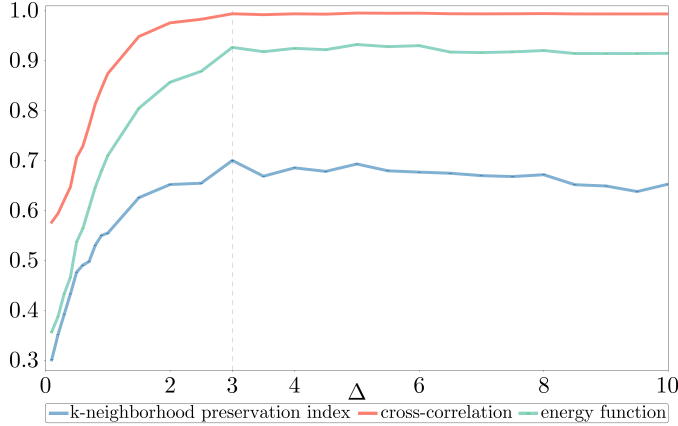


Fig. 6. Impact of varying the grid dimensions to the quality of the produced layouts. The best results are attained when the grid dimensions are related to the distribution of the input projection.

of processing large datasets. In this test, we have selected 10 datasets from the *UCI Machine Learning Repository*, varying the sizes up to 130,000 instances. The employed datasets are detailed in the second part of Table 1. Figure 7 summarizes the results. To allow a fair comparison, DGrid and SSM are both implemented in Java. Besides the boxplots for the DGrid and the SSM techniques, the figure shows individual boxplots for the projection and the grid assignment steps. In this example, we are using LAMP to project the data. On average, the DGrid is almost two orders of magnitude faster than the SSM. Still, better results can be obtained if a faster projection technique is employed (the projection step dominates the process). Considering the tested techniques, DGrid presents the best tradeoff between running times and quality of the produced grids, placing it among the state-of-the-art techniques for generating distance preserving grids from large datasets.

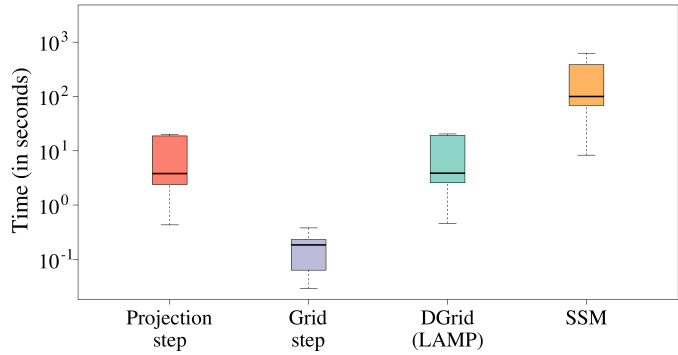


Fig. 7. Running times boxplots. DGrid is almost two orders of magnitude faster than the SSM technique, and the projection phase dominates its running times. We have removed the other technique from this comparison since they are not capable of processing large datasets.

## 4.2 Usage Scenarios

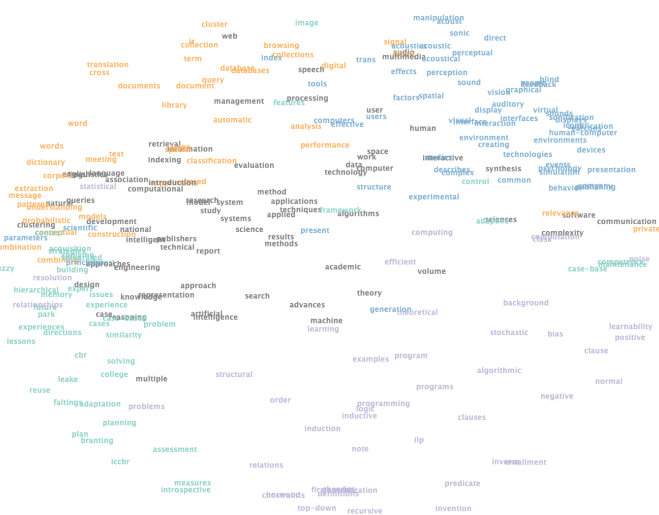
Currently, dimension reduction or multidimensional projection techniques are the de facto strategies to analyze distance or neighborhood patterns in multidimensional datasets, such as groups of similar instances and the frontiers between groups. Although prevalent, the typical scatterplot visual metaphor to display a projection, customarily presents problems with occlusion, especially when more elaborate icons are used to represent information about the data instances. Figure 8 shows a projection of the most relevant terms of a scientific paper collection containing papers of four

different areas, case-based reasoning, inductive logic programming, information retrieval, and sonification. To extract these terms, we use the topic extraction technique presented in [5], getting 50 terms for each group of papers, resulting in 186 terms (some terms occur in multiple groups). Each term is then represented by a vector computed by getting the transpose of the usual bag-of-words representation of the papers (terms are instances, papers are dimensions), and the distance among terms is calculated using the cosine dissimilarity.

In this figure, the icons are the actual terms, and color reflects the area of papers they better represent. Green terms denote case-based reasoning papers, orange, information retrieval, blue, sonification, and purple, inductive logic programming. Terms in gray are the ones that belong to more than one group of papers. Even for a small number of terms, the resulting visual representation is difficult to understand due to the significant overlap. In this scenario, grids are better choices as the overlap is eliminated, resulting in a more readable representation. Figure 9(b) depicts the resulting grid of the projection of Figure 8. In this layout, some terms that were hidden by the overlap in the projection are visible. Also, some interesting patterns are easier to recognize. For instance, most of the gray terms compose a frontier between the different groups of terms since they are not specific to any area. However, some of them are better suited to particular groups, such as “retrieval” among the information retrieval terms, or to some groups, such as “multimedia” located between information retrieval and sonification terms. This gives an overall picture of terms’ importance and uniqueness for different areas and what is shared among areas.

In general, grids present some advantageous characteristics over multidimensional projections when the input dataset does not represent clear groups, resulting in more readable layouts. However, there are cases where datasets have clear groups, which, through a proper technique, can result in projections that support analysis not supported by a grid, e.g., the distance between groups. Figure 9(a) presents an example of such a projection. This is a projection of the same scientific papers collection used in Figure 8, but in this case, the circles represent the papers. Green points denote case-based reasoning papers, orange, information retrieval, blue, sonification, and purple, inductive logic programming. Different groups and sub-groups of points can be observed, with different sizes and densities. Also, frontiers between (sub)groups and their magnitude are visible, representing the difference between the papers’ areas. Notice that this is only true for techniques with good global preservation of distances, but might not mean anything for techniques focused on local preservation, such as the t-SNE [34]. In this example, we use the Least-Square Projection (LSP) [35] since it presents a good balance between local and global preservation.

Figure 9(b) shows the resulting grid. Although some information is clearer in the grid representation due to the overlap elimination, for instance, the outliers orange points inside the group of green points, the distance between groups is lost. One simple solution to this problem is to add “dummy” points in the projection, i.e., points to represent empty spaces before assigning the projection to a grid. Here we devise a simple yet effective solution to add such points into low-density areas of a projection. In this process, we first calculate the average  $k$ -distance of the projection points. The  $k$ -distance of point  $p_i$  is the distance of  $p_i$  to its  $k^{\text{th}}$  nearest neighbor. Then we compute the candidate “dummy” points, uniformly spacing them on the projection according to the average  $k$ -distance, but only adding points in which the minimum



(a) Scatterplot-based visual metaphor.



(b) Distance preserving grid metaphor.

Fig. 8. Different distance-based visual representations of the most important terms of a scientific paper collection containing papers of four different areas. In (a) the usual scatterplot-based visual metaphor to represent multidimensional projections is used. In (b), the distance-preserving grid layout is employed. Even for a small number of terms, the scatterplot-based metaphor is difficult to understand due to the significant overlap. The grid representation eliminates the overlap, resulting in a more readable representation.

distance to the projection points is larger than the  $k$ -distance. Figure 9(c) presents the projection with the “dummy” points (white points), and Figure 9(d) the resulting grid. In the “dummy” grid, the density or size of the groups is better represented, and “outlier” points are easier to detect if compared to the original projection. Besides, the shape of the projection is preserved while the overlaps are eliminated. However, the resulting grid with “dummy” points has many more rows and columns than the grid without such points, being less effective in terms of space utilization. In this example, this is not a problem as the employed icons to represent papers are very simple (only color). However, poor space usage can be a limitation when icons are richer and convey more information, such as images (discussed in the following section). So, the choice of adding “dummy” points or not rely on the intended application and if the input dataset has clear groups or not.

Worth noting that it is not our goal to present our approach

as an overlap elimination approach for projections techniques or to produce grids with gaps. However, it can be used for that end. We are only presenting this approach to add “dummy” points as a simple solution if projections without overlapping are the goal given that for some applications, gaps can be beneficial [23].

## 5 USE CASE: EXPLORING PHOTO COLLECTIONS

Exploring image collections have been one of the main applications for distance preserving grids, with a positive impact on image retrieval tasks [36]. In this section, we present a strategy using DGrid to explore photo collections that allow users to control the semantics of the similarity between images and to navigate collections into different levels of detail. Here, to compose a usage scenario, we employ the Photographer dataset [37], composed of 180,193 photos taken by 41 well-known photographers. We extract 4 different sets of features from this dataset, representing: (1) color, using LaB color features; (2) texture, using Gabor filters [38]; (3) borders, using the HoG technique [39]; and (4) the presence of objects, using a pre-trained convolutional neural network [40] that classifies images into 1,000 different object categories.

To allow manipulating the semantics of the similarity between photos, we use the feature fusion strategy defined in [41], employing grids instead of multidimensional projections as the visual representations. The idea is to combine different sets of features describing the photos, allowing users to control in real-time how much each distinct feature contributes to the similarity. It is a two-step approach. In the first step, a sample of photos is extracted, and a grid created. This enables users to interactively merge and visually inspect the result, seeking the weighted combination that best approaches his/her point of view regarding similarity. In the second step, the combination weights defined in the first step are used to determine the similarity of the entire photo collection, and a complete grid is generated, which can then be explored into different levels of detail. In this paper, to create the photo sample, we get 200 photos of each different set of features, ensuring we have at least 5 photos of each photographer (800 photos in total).

Figure 10 shows two examples of sample grids using different weighted feature combinations. To visually support the real-time exploration of multiple combinations, the widget, shown in the bottom-right of the grids, is used. In this widget, the weights for the combination are defined based on the closeness of the “orange” dial and the anchors representing each feature [41]. In Figure 10(a), the combination assigns a substantial weight on the “object” feature indicated by the closeness of the dial to the anchor representing it. As a result, the semantics of the similarity mostly reflect the presence of objects, and the produced grid is organized considering the detected objects. For instance, photos of people are placed towards the right and photos of buildings towards the left. Figure 10(b) presents a new sample grid with the addition of the color feature to the combination. A smooth transition from colored to black-and-white photos can now be observed while groups of photos containing specific scenes or objects can also be found, e.g., people, buildings or landscapes.

Once the proper combination has been defined according to the users' point of view, a grid representing the complete photo collection is built. In this example, given the aspect ratio of the visual area (paper size), we set  $\Delta = 11/8.5$ , resulting in a photo grid with 482 rows and 374 columns. Since this is too much to present at once, we perform a grid compression. In this process, we convolute the grid with a  $R \times S$  mask merging the covered cells into one

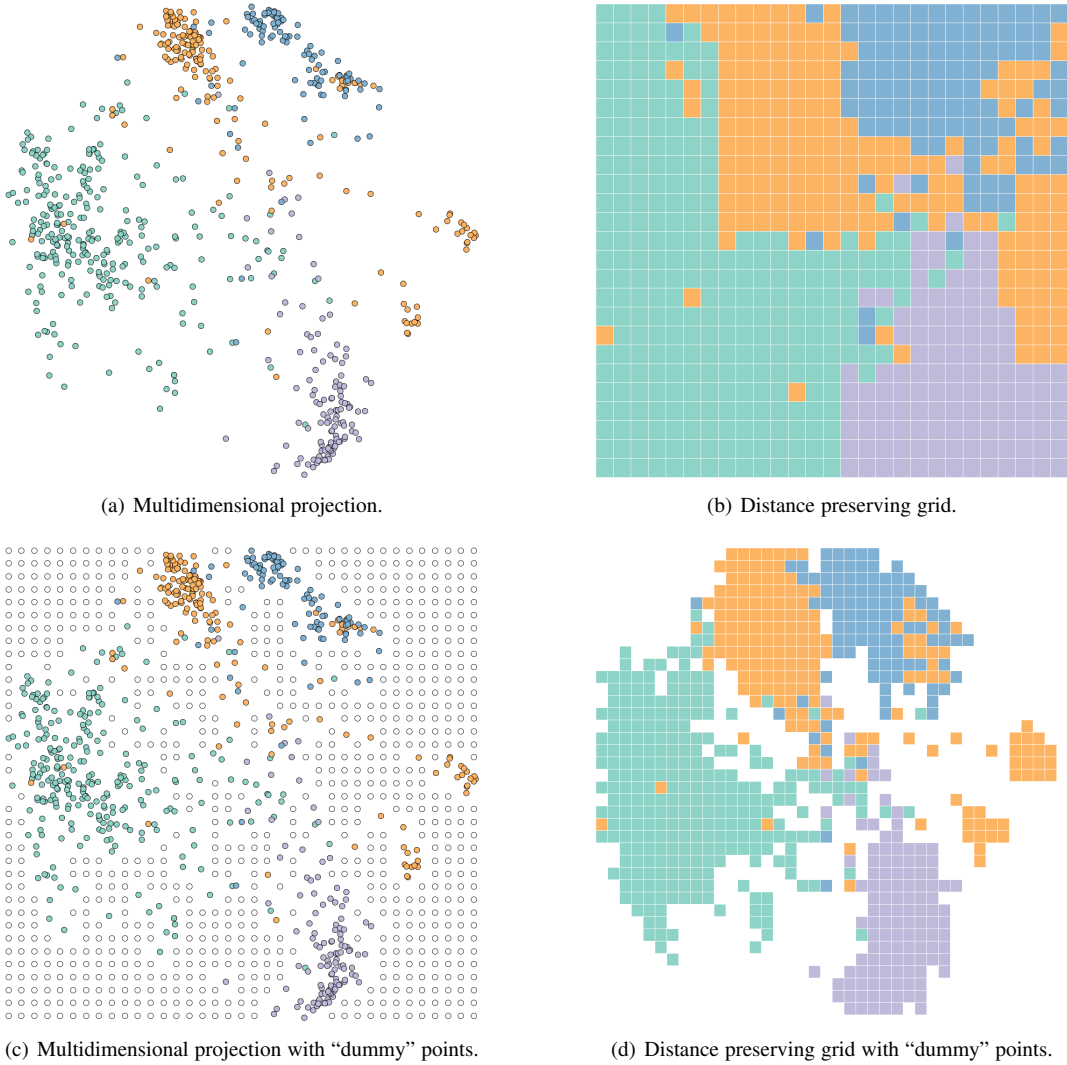
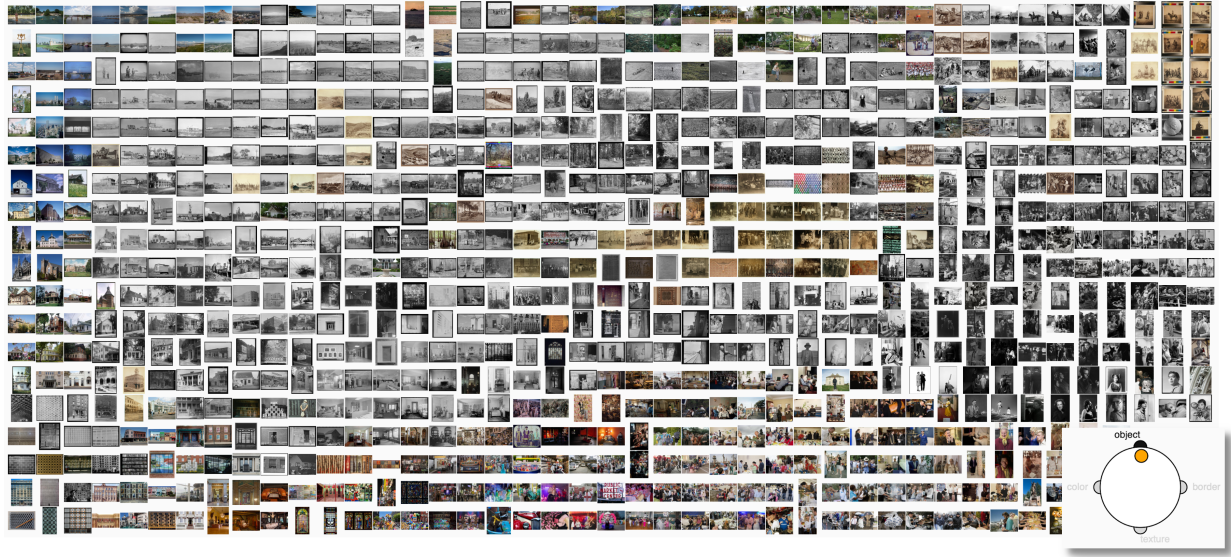


Fig. 9. For datasets presenting clear groups, multidimensional projections can aid in analytical tasks not supported by grid layouts, such as the analysis of distances between groups. In (a), a projection of a collection of scientific papers of four distinct areas is presented, in (b), the resulting grid. Given the nature of the grid representation, the space between groups is lost. One simple solution is to add “dummy” points, representing spaces in a projection before assigning it to a grid. In (c), the white circles are the “dummy” points, and in (d), the resulting grid is shown. The visual representation is very close to the original projection, but the density or size of the groups is better represented. Also, “outlier” points are easier to detect if compared to the original projection.

single cell, thus dividing the number of rows by  $R$  and the number of columns by  $S$ . In the compact layout, the cells are represented by the photo closest to the center of the  $R \times S$  mask. The mask  $R \times S$  defines the level of detail of the compact representation. Changing its size allows the composition of photo grids with different levels of abstraction, from a coarse representation to a more detail view. Figure 11 presents a compressed photo grid with 96 rows and 75 columns using a  $5 \times 5$  mask. To generate this grid, we use the weights defined in Figure 10(b), organizing the photos by the presence of objects and color. In the final grid, a smooth transition of colored to black-and-white photos, similar to the sample grid, can be observed, and groups of photos containing specific scenes or objects can also be found. For instance, the grid’s top-right corner presents mainly black-and-white landscape photos (we zooming-in a small area to easier the visualization). Notice that the quality of the final grid depends on the quality of the features used to represent the photos, which is a complex process and has been the concern of multiple areas of research. The discussion of what composes good features is beyond the scope of this paper.

To navigate this grid into multiple levels of detail, users select a particular photo, expanding the compressed grid to show all the photos it represents. In this case, by expanding all the cells belonging to the same row or same column of the selected photo, defining a process that preserves context. In [9] a similar application was presented. However, they use a hierarchical clustering approach to group the instances, showing representatives of the groups. The user can then navigate by clicking on the representatives, displaying new grids containing the elements (or representatives) inside the groups. Therefore, losing the context whenever a zoom-in operation is executed.

Since the similarity between images is on the eye of the viewer, allowing users to control the semantics of the employed similarity based on combinations of different features renders a powerful and flexible mechanism to fast browse photo collections. Notice that this application is only possible given the high efficiency of DGrid to derive grids in real-time, a trait not found in the current state-of-the-art techniques in the distance preserving grid layouts.



(a) Sample grid organizing photos according to the presence of objects.



(b) Sample grid organizing photos considering both the color component and the presence of objects.

Fig. 10. Examples of sample grids using different feature combinations. In both images, the widget in the bottom-right helps in controlling such combination and indicates the importance of each feature. In (a), the combination assigns a large weight to the “object” feature, resulting in a grid that mostly reflects the presence of objects. In (b), the “color” feature is added to the combination, and the resulting grid organizes the photos from colored to black-and-white images while groups of photos containing specific scenes or objects can also be observed.

## 6 DISCUSSION AND LIMITATIONS

The space partition strategy presented in Algorithm 1 shares similarities with the kd-tree technique [42]. In both cases, the recursive process of bisecting the space into partitions and sub-partitions constructs complete binary trees. The difference is that the kd-tree only considers the spatial position of the points in this process, whereas our approach incorporates the number of rows and columns to it. As a result, our technique can create grids with an arbitrary number of rows and columns while the kd-tree can only create squared grids that are power-of-two [12]. The same applying to the NMAP technique [21], as discussed in Section 2.

Regarding the computational complexity, the DGrid has two distinct steps. The projection and the space partition. Different techniques can be used in the first step, with different complexities. Here we use the t-SNE, which is  $O(N^2)$  and the LAMP, which is

$O(\min\{m^2N^{\frac{3}{2}}, mN^2\})$ , where  $m$  is the number of dimensions of the dataset. Recalling that in our algorithm every time a partition is bisected, its instances are sorted according to the  $x$  or  $y$  coordinates. If an  $O(N \log N)$  sorting algorithm is used, the computational complexity of the space partition step is  $O(N \log^2 N)$ . However, it can be reduced to  $O(N \log N)$  if a pre-sorting strategy is used [43]. In any case, the overall computational complexity is dominated by the projection process, which is confirmed by the running times (see Figure 7). If a faster approach is required, changing the projection technique is an option, for instance, PLMP [31] is  $O(N)$ , but the quality of the obtained grids will be penalized.

The way DGrid was conceived only allows it to generate regular grids, KS and IsoMatch are more flexible. Since they are based on assignment processes, they can map data instances into non-regular domains. However, they are computationally expensive,  $O(N^3)$ . For regular grids, the DGrid is much faster, attaining similar, or even

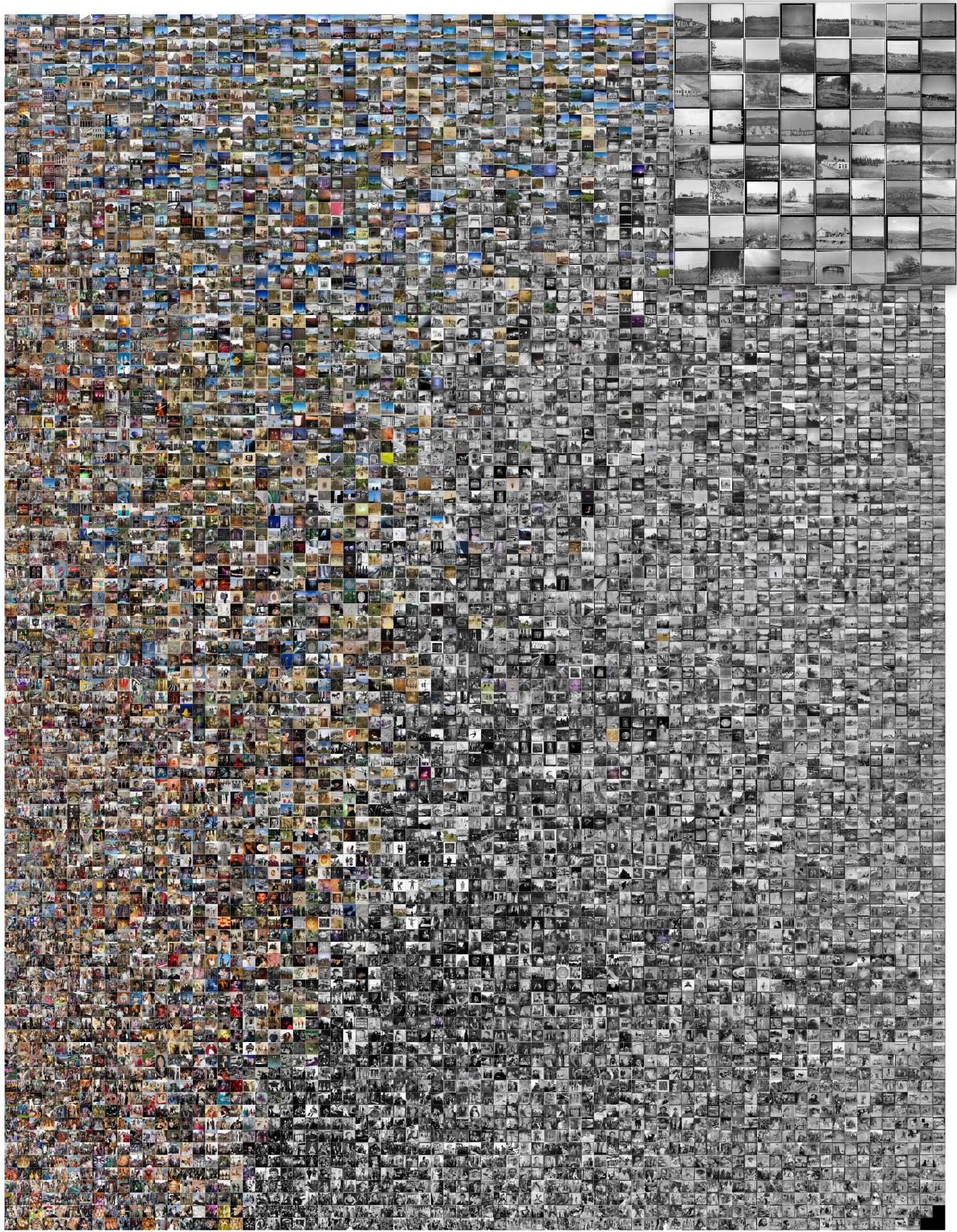


Fig. 11. Compressed photo grid of the Photographers dataset. Since similar weights are assigned to the color and presence of objects features (see Figure 10(b)), a smooth transition of colored to black-and-white photos can be observed (from left to right) while groups of photos containing specific scenes or objects can be found, as shown in the zooming-in part on the top-right corner that mainly contains black-and-white landscape photos.

better results considering different quality metrics, rendering DGrid a very attractive technique for processing large datasets. Also, in our technique, the bisection lines are orthogonal or parallel among themselves. However, it is possible to use arbitrary orientations for such bisectors, potentially resulting in better grids. However, this increases the complexity of our approach and, consequently, its running times. Something that conflicts with our goal of keeping our technique as simple as possible.

Another possibility to potentially improve the technique is to use a strategy to find the best (orthogonal) partitioning point. To compare, we implemented and tested the Jenks' Natural Break [44] strategy to find the best partition point. The Natural Break is a clustering approach that partitions univariate datasets to reduce the variance within-cluster and maximize the variance between clusters. On average, no improvement was observed in terms of cross-correlation ( $\overline{CC} = 0.78$  using LAMP), energy function ( $\overline{E_p} = 0.63$  using LAMP), and neighborhood preservation index ( $\overline{NP} = 0.47$  using t-SNE). This is an expected outcome since the effectiveness of the Natural Break is reduced, given the reduced number of possibilities for a cut. Considering a bisection to produce a (sub)grid with  $r$  rows and  $r$  columns, we have only  $r$  possible horizontal cuts and  $s$  possible vertical cuts. So, there is no much room for defining the best partition of the points. Besides, the technique gets two orders of magnitude slower, again conflicting with our goal of keeping our approach as simple and fast as possible.

Depending on the marginal distribution of the  $x$  and  $y$ -coordinates of the input projection, our approach will produce artifacts in the resulting grids. For instance, if the input projection is misaligned with the target grid (e.g., a rhombus-shaped projection), artifacts will be created, especially in the corners of the grid. The projection rotation strategy presented in Section 3.3 reduces such problems, but irregularly shaped projections are still a problem. Also, datasets with well-defined groups, and therefore, resulting in projections with marginal distributions that deviate from the uniformity will result in grids with low-quality cells since “border” data instances belonging to different groups are approximated. However, this is a bottleneck we observed in all distance preserving grid techniques we tested given their nature of using the available area as much as possible. As a potential solution, we present a strategy to add “dummy” points representing empty spaces in the projection before assigning it to a grid. The result is a grid that more faithfully represents groups and frontiers between groups, but at a price of waisting visual area, conflicting with our goal of using the visual space as much as possible.

Finally, our goal was to define a technique to create grids that preserve distance relationships, using a two-step approach involving multidimensional projections and a grid cell index calculation strategy. Thereby, the multidimensional projection is just a step in our approach. However, our grid cell index calculation strategy (see Algorithm 1) can be used to map any point cloud to a grid while preserving the distance among the points. So, virtually, any point-based technique, e.g., RadViz [45] and Star Coordinates [46], not only multidimensional projection, can benefit from our strategy to be mapped to an orthogonal regular grid.

## 7 CONCLUSION

In this paper, we proposed a novel approach for generating grid layouts that preserve distance information, called *Distance-preserving Grid (DGrid)*. DGrid is a two-step approach that combines a projection technique with an assignment strategy

to create orthogonal regular grids. The set of comparisons we provide shows that DGrid outperforms the existing state-of-the-art techniques considering different quality metrics, being almost two orders of magnitude faster than the fastest existing technique. The quality of the produced layouts combined with the low computational cost render DGrid one of the most attractive methods for generating distance preserving grid layouts.

## REFERENCES

- [1] L. G. Nonato and M. Aupetit, “Multidimensional projection for visual analytics: Linking techniques with distortions, tasks, and layout enrichment,” *IEEE Transactions on Visualization and Computer Graphics*, vol. 25, no. 8, pp. 2650–2673, Aug 2019.
- [2] J. Poco, D. M. Eler, F. V. Paulovich, and R. Minghim, “Employing 2d projections for fast visual exploration of large fiber tracking data,” *Computer Graphics Forum*, vol. 31, no. 3pt2, pp. 1075–1084, 2012.
- [3] Y. Chen, J. Hua, M. Dong, and L. Wang, “Exemplar-based visualization of large document corpus (infovis2009-1115),” *IEEE Transactions on Visualization & Computer Graphics*, vol. 15, pp. 1161–1168, 09 2009.
- [4] W. Cui, Y. Wu, S. Liu, F. Wei, M. X. Zhou, and H. Qu, “Context-preserving, dynamic word cloud visualization,” *IEEE Comput. Graph. Appl.*, vol. 30, no. 6, pp. 42–53, Nov. 2010.
- [5] F. V. Paulovich, F. M. B. Toledo, G. P. Telles, R. Minghim, and L. G. Nonato, “Semantic wordification of document collections,” *Comput. Graph. Forum*, vol. 31, no. 3pt3, pp. 1145–1153, Jun. 2012.
- [6] E. Gomez-Nieto, F. S. Roman, P. Pagliosa, W. Casaca, E. S. Helou, M. C. F. de Oliveira, and L. G. Nonato, “Similarity preserving snippet-based visualization of web search results,” *IEEE Transactions on Visualization and Computer Graphics*, vol. 20, no. 3, pp. 457–470, March 2014.
- [7] H. Strobelt, M. Spicker, A. Stoffel, D. Keim, and O. Deussen, “Rolled-out wordles: A heuristic method for overlap removal of 2d data representatives,” *Computer Graphics Forum*, vol. 31, no. 3pt3, pp. 1135–1144, 2012.
- [8] R. D. Pinho, M. C. Oliveira, and A. Andrade Lopes, “An incremental space to visualize dynamic data sets,” *Multimedia Tools Appl.*, vol. 50, no. 3, pp. 533–562, Dec. 2010.
- [9] O. Fried, S. DiVerdi, M. Halber, E. Sizikova, and A. Finkelstein, “Isomatch: Creating informative grid layouts,” *Comput. Graph. Forum*, vol. 34, no. 2, pp. 155–166, May 2015.
- [10] N. Quadrant, A. J. Smola, L. Song, and T. Tuytelaars, “Kernelized sorting,” *IEEE Transactions on Pattern Analysis and Machine Intelligence*, vol. 32, no. 10, pp. 1809–1821, Oct 2010.
- [11] G. Strong and M. Gong, “Data organization and visualization using self-sorting map,” in *Proceedings of Graphics Interface 2011*, ser. GI ’11. School of Computer Science, University of Waterloo, Waterloo, Ontario, Canada: Canadian Human-Computer Communications Society, 2011, pp. 199–206.
- [12] ———, “Self-sorting map: An efficient algorithm for presenting multimedia data in structured layouts,” *Trans. Multi.*, vol. 16, no. 4, pp. 1045–1058, Jun. 2014.
- [13] W. S. Torgerson, “Multidimensional scaling of similarity,” *Psychometrika*, vol. 30, no. 4, pp. 379–393, Dec 1965.
- [14] L. van der Maaten and G. Hinton, “Visualizing High-Dimensional Data Using t-SNE,” *Journal of Machine Learning Research*, vol. 9, pp. 2579–2605, Nov. 2008.
- [15] J. B. Tenenbaum, V. d. Silva, and J. C. Langford, “A global geometric framework for nonlinear dimensionality reduction,” *Science*, vol. 290, no. 5500, pp. 2319–2323, 2000.
- [16] P. Joia, D. Coimbra, J. A. Cuminato, F. V. Paulovich, and L. G. Nonato, “Local affine multidimensional projection,” *IEEE Transactions on Visualization and Computer Graphics*, vol. 17, no. 12, pp. 2563–2571, Dec. 2011.
- [17] N. Cao, Y. R. Lin, and D. Gotz, “Untangle map: Visual analysis of probabilistic multi-label data,” *IEEE Transactions on Visualization and Computer Graphics*, vol. 22, no. 2, pp. 1149–1163, Feb 2016.
- [18] T. Kohonen, “Neurocomputing: Foundations of research,” J. A. Anderson and E. Rosenfeld, Eds. Cambridge, MA, USA: MIT Press, 1988, ch. Self-organized Formation of Topologically Correct Feature Maps, pp. 509–521.
- [19] C. M. Bishop, M. Svensén, and C. K. I. Williams, “Gtm: The generative topographic mapping,” *Neural Computation*, vol. 10, no. 1, pp. 215–234, Jan 1998.

[20] Y. Weiss, A. Torralba, and R. Fergus, "Spectral hashing," in *Advances in Neural Information Processing Systems 21*, D. Koller, D. Schuurmans, Y. Bengio, and L. Bottou, Eds. Curran Associates, Inc., 2009, pp. 1753–1760.

[21] F. S. L. G. Duarte, F. Sikansi, F. M. Fatore, S. G. Fadel, and F. V. Paulovich, "Nmap: A novel neighborhood preservation space-filling algorithm," *IEEE Transactions on Visualization and Computer Graphics*, vol. 20, no. 12, pp. 2063–2071, Dec 2014.

[22] B. Shneiderman, "Tree visualization with tree-maps: 2-d space-filling approach," *ACM Trans. Graph.*, vol. 11, no. 1, pp. 92–99, Jan. 1992.

[23] W. Meulemans, J. Dykes, A. Slingsby, C. Turkay, and J. Wood, "Small multiples with gaps," *IEEE Transactions on Visualization and Computer Graphics*, vol. 23, no. 1, pp. 381–390, Jan 2017.

[24] T. C. Koopmans and M. Beckmann, "Assignment problems and the location of economic activities," *Econometrica*, vol. 25, no. 1, pp. 53–76, 1957.

[25] H. W. Kuhn, "The hungarian method for the assignment problem," *Naval Research Logistics Quarterly*, vol. 2, no. 1-2, pp. 83–97, 1955.

[26] M. van Kreveld and B. Speckmann, *On Rectangular Cartograms*. Berlin, Heidelberg: Springer Berlin Heidelberg, 2004, pp. 724–735.

[27] E. Raisz, "The rectangular statistical cartogram," *Geographical Review*, vol. 24, no. 2, pp. 292–296, 1934.

[28] G. McNeill and S. A. Hale, "Generating tile maps," *Comput. Graph. Forum*, vol. 36, no. 3, pp. 435–445, Jun. 2017.

[29] J. Wood, J. Dykes, and A. Slingsby, "Visualisation of origins, destinations and flows with od maps," *The Cartographic Journal*, vol. 47, no. 2, pp. 117–129, 2010.

[30] D. Eppstein, M. van Kreveld, B. Speckmann, and F. Staals, "Improved grid map layout by point set matching," in *2013 IEEE Pacific Visualization Symposium (PacificVis)*, Feb 2013, pp. 25–32.

[31] F. V. Paulovich, C. T. Silva, and L. G. Nonato, "Two-phase mapping for projecting massive data sets," *IEEE Transactions on Visualization and Computer Graphics*, vol. 16, no. 6, pp. 1281–1290, Nov. 2010.

[32] S. G. Fadel, F. M. Fatore, F. S. Duarte, and F. V. Paulovich, "Loch: A neighborhood-based multidimensional projection technique for high-dimensional sparse spaces," *Neurocomputing*, vol. 150, no. Part B, pp. 546 – 556, 2015.

[33] M. Lichman, "UCI machine learning repository," 2013. [Online]. Available: <http://archive.ics.uci.edu/ml>

[34] M. Wattenberg, F. Viégas, and I. Johnson, "How to use t-sne effectively," *Distill*, 2016. [Online]. Available: <http://distill.pub/2016/misread-tsne>

[35] F. V. Paulovich, L. G. Nonato, R. Minghim, and H. Levkowitz, "Least square projection: A fast high-precision multidimensional projection technique and its application to document mapping," *IEEE Transactions on Visualization and Computer Graphics*, vol. 14, no. 3, pp. 564–575, May 2008.

[36] K. Schoeffmann and D. Ahlstrom, "Similarity-based visualization for image browsing revisited," in *2011 IEEE International Symposium on Multimedia*, Dec 2011, pp. 422–427.

[37] C. Thomas and A. Kovashka, "Who's behind the camera? identifying the authorship of a photograph," *CoRR*, vol. abs/1508.05038, 2015.

[38] L. Chen, G. Lu, and D. Zhang, "Effects of different gabor filter parameters on image retrieval by texture," in *Proceedings of the 10th International Multimedia Modelling Conference*, ser. MMM '04. Washington, DC, USA: IEEE Computer Society, 2004, pp. 273–.

[39] N. Dalal and B. Triggs, "Histograms of oriented gradients for human detection," in *In CVPR*, 2005, pp. 886–893.

[40] Y. Jia, E. Shelhamer, J. Donahue, S. Karayev, J. Long, R. Girshick, S. Guadarrama, and T. Darrell, "Caffe: Convolutional architecture for fast feature embedding," in *Proceedings of the 22Nd ACM International Conference on Multimedia*, ser. MM '14. New York, NY, USA: ACM, 2014, pp. 675–678.

[41] G. M. Hilasaca and F. V. Paulovich, "Visual feature fusion and its application to support unsupervised clustering tasks," *Information Visualization*, vol. 0, no. 0, pp. 1–17, 2019.

[42] J. L. Bentley, "Multidimensional binary search trees used for associative searching," *Commun. ACM*, vol. 18, no. 9, pp. 509–517, Sep. 1975.

[43] R. A. Brown, "Building a balanced  $k$ -d tree in  $o(kn \log n)$  time," *Journal of Computer Graphics Techniques (JCGT)*, vol. 4, no. 1, pp. 50–68, March 2015.

[44] G. F. Jenks, "The data model concept in statistical mapping," *International Yearbook of Cartography*, vol. 7, pp. 186–190, 1967.

[45] P. Hoffman, G. Grinstein, and D. Pinkney, "Dimensional anchors: A graphic primitive for multidimensional multivariate information visualizations," ser. NPIVM 99. New York, NY, USA: Association for Computing Machinery, 1999, pp. 9–16.

[46] E. Kandogan, "Star coordinates: A multi-dimensional visualization technique with uniform treatment of dimensions," in *In Proceedings of the IEEE Information Visualization Symposium, Late Breaking Hot Topics*, 2000, pp. 9–12.